Coulomb explosion of 173-MeV HeH^+ ions traversing carbon foils

M. P. Carpenter, R. W. Dunford, D. S. Gemmell, T. Graber,* R. V. F. Janssens, E. P. Kanter, J. A. Nolen, Jr, and Z. Vager†

Physics Division, Argonne National Laboratory, Argonne, Illinois 60439

(Received 26 July 1996)

The Coulomb explosion of 173-MeV HeH^+ molecular ions traversing thin carbon foils has been measured for foil thicknesses ranging from 2 to 200 $\mu g/cm^2$. In contrast with measurements at lower energies, the energy spectra for protons observed emerging in the incident beam direction show distinct components that correspond to the partner helium ions being in charge states 0, 1, and 2. From an analysis of the variation of the yields of these components as functions of the target thickness, we extract electron-loss cross sections that are in good agreement with theoretical estimates. ''Wake effects'' that increase with increasing target thickness are observed as asymmetries in the yields and energy shifts for ''backward-going'' as compared to ''forward-going'' protons. [S1050-2947(97)08203-6]

PACS number(s): 34.50.Bw, 34.90.+q, 34.70.+e

I. INTRODUCTION

When a fast ($v > v_0 = e^2/\hbar$) molecular projectile impinges on a solid target, many or all of the electrons that bind the projectile are torn off during passage through the first few atomic layers as a result of collisions with target electrons. The molecular constituents then dissociate, undergoing a ''Coulomb explosion'' as they separate due to their mutual coulomb repulsion.

The Coulomb explosions of light molecular ions have been thoroughly studied for projectile energies extending up to a few MeV (see, for example, Refs. [1–8]). The time during which electron stripping from the projectile occurs is generally on the order of 0.01 fs and this is short compared to the characteristic periods for vibration ($\sim$10 fs) and rotation ($\sim$1000 fs) in the projectile. Thus the Coulomb explosion essentially takes a ''snapshot'' of the positions of the molecular constituents at the point of entry into the solid. Furthermore, the energies associated with internal molecular excitation are small compared to the Coulomb-explosion energy, which is typically 10's or even 100's of eV. This means that the final kinetic energies of the dissociated molecular fragments are determined principally by their initial relative positions in the molecule and are little influenced by the relative momentum distribution within the molecule. These initial positions are themselves governed by the way in which internal vibrational states are populated.

The Coulomb repulsion between the fragments inside the foil is screened by the electrons in the foil, and the screening distance is on the order of v/ω_p, where v is the beam velocity and ω_p is the plasmon frequency for the target electrons ($\hbar\omega_p \approx 25$ eV for carbon [9]). Thus, for projectile energies greater than about 100 keV per nucleon, the screening distance is larger than the initial fragment separations and the repulsive force is approximately Coulombic. Classically, for the case of a diatomic projectile dissociating via a purely Coulombic force, the time for the internuclear separation of the two fragments to grow to r from an initial value of r_0 is given by [5]

$$t(r/r_0) = t_0 f(r/r_0), \tag{1}$$

where

$$t_0 = [\mu r_0^3/(2Q_1Q_2e^2)]^{1/2}, \tag{2}$$

and

$$f(x) = \sqrt{x}\sqrt{x-1} + \ln(\sqrt{x} + \sqrt{x-1}). \tag{3}$$

Here μ is the reduced mass for the two fragments and Q_1 and Q_2 are their ionic charge states. [We are making the assumption here that the fragments are stationary when the Coulomb explosion starts ($t=0$).] Thus, t_0 is a characteristic time for the Coulomb explosion: it is the time it takes for the two fragments to increase their initial separation by 23% and is typically about 1 fs. Since in many experiments the projectile dwell times inside the foil targets are also around 1 fs, it is apparent that the Coulomb explosion typically does not increase the distance between molecular fragments by more than a few percent during traversal of the foil.

Studies on the penetration of fast molecular ions through solids present a challenge to the understanding of penetration phenomena in general. Although present-day understanding of effects associated with fast monatomic ions traversing solids (energy loss, multiple scattering, charge-state distributions, etc.) has reached a high level, the same cannot be said for similar effects observed in the passage of a compact cluster of ions as when molecular projectiles are employed. Some progress has, however, been made on several of the rather difficult problems involved with a theoretical description of cluster penetration phenomena (see, for example, Refs. [10–14].

The work reported here was undertaken with a view to extending the study of cluster penetration effects to projectile velocities substantially higher than those previously used. For this we chose the projectile HeH^+ (familiar from several

*Present address: Advanced Photon Source, Argonne National Laboratory.

†Permanent address: Weizmann Institute of Science, Rehovoth, Israel.

 © 1997 The American Physical Society

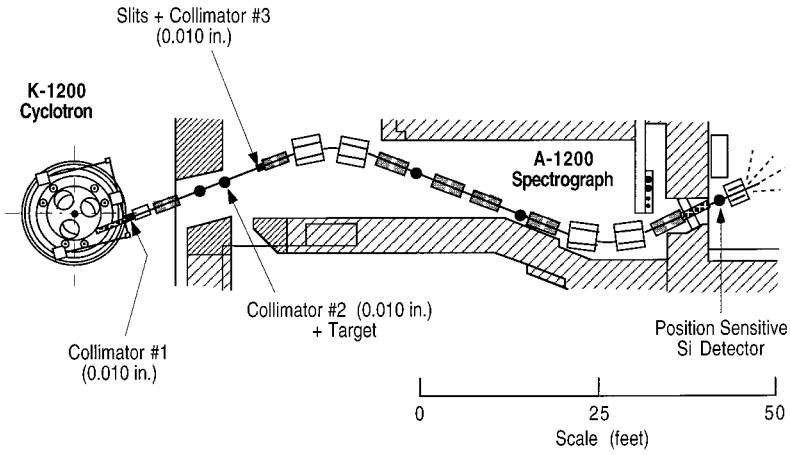

FIG. 1. Schematic diagram showing the experimental arrangement.

earlier studies) and an energy of 173.25 MeV (34.65 MeV per nucleon), which corresponds to $\beta = v/c = 0.27$.

At such high projectile velocities, several differences can be anticipated when comparison is made to the situation at lower velocities. For example, one expects the opening angles for the Coulomb-explosion fragments to be reduced in inverse proportion to the beam velocity and the energy shifts engendered by the Coulomb explosion to be increased in proportion to the beam velocity. Also, relativistic effects begin to play a role. The aligning influence of the ''wake'' forces [2,12,15] is reduced because of the extension of the wake wavelength ($\lambda \approx 2\pi v/\omega_p$) and because of the smaller time in the foil during which the wake forces can operate. Also, since the electron capture and loss cross sections are lower, the fragments travel further into the foil before charge-state equilibrium is achieved.

II. EXPERIMENTAL ARRANGEMENT

A schematic diagram of the experimental arrangement is given in Fig. 1. The measurements were conducted at the National Superconducting Cyclotron Laboratory (NSCL) at Michigan State University. HeH^+ ions were produced in an electron-cyclotron-resonance (ECR) ion source and accelerated to 173.25 MeV with the K-1200 superconducting cyclotron [16]. An ion beam with an intensity of ~ 5 nA was extracted and then tightly collimated (divergence ± 0.05 mrad) onto a carbon-foil target mounted over a 0.010-in.-diam hole in a 0.005-in.-thick Ta disk (this hole served as the final aperture in collimating the incident beam).

Projectile fragments emerging from the foil within 0.2 mrad of the incident beam direction passed through another 0.010-in.-diam collimator and then into the superconducting A1200 spectrograph, which was operated in dispersive mode [17]. Analyzed ionic fragments transmitted through the spectrograph were recorded with a 500-μm-thick position-sensitive silicon detector (PSD) located at the focal plane.

Carbon-foil targets of a variety of thicknesses were mounted on a remotely positionable ''target ladder.'' The foils were obtained commercially and were prepared by standard methods involving vacuum deposition from a carbon arc onto a glass substrate. Their nominal thicknesses were checked by α-particle energy-loss techniques and were found to be accurate to about 5%. Previous experience in our laboratory indicates that these foils do not give rise to any observable ion channeling effects. Thus for the present purpose, they may be regarded as being amorphous (although in actual fact they are probably polycrystalline with microcrystal sizes much smaller than our target beam-spot diameter of 0.010 in.). The foil densities are estimated to be close to 2.0 g/cm^3. For each new target that was positioned in the beam, the angular pattern of the exiting fragments under study was recentered on the collimator in front of the A1200 by means of minor adjustments to both horizontal and vertical magnetic steerers in the beam line. It was expected that any molecular breakup occurring as a result of beam interactions with the Ta target holder would give rise to fragments suffering such large energy losses and/or angular deflections that they would not pass through the spectrometer system, which was highly selective in both energy and angle. This expectation was checked by running a test with an empty target holder and verifying that there were no counts observed in the detector at the end of the spectrometer. Similar reasoning led to the expectation that the measurements would not be adversely affected by the use of a small (0.010 in.) aperture in the the Ta aperture at the entrance to the spectrometer and this was checked and verified by making measurements with a series of collimating aperture sizes.

III. RESULTS AND DISCUSSION

Figure 2 shows a set of energy spectra for protons arising from beam fragmentation in carbon-foil targets whose areal densities range from 2 to 200 micrograms per square centimeter (thicknesses ranging from ~ 100 to $\sim 10\,000$ Å). These spectra were derived from position spectra recorded with the PSD. The factor translating the positional scale into an energy scale was determined by recording a series of spectra for magnetic field settings in the A1200 both slightly above and slightly below the settings that centered the spectra on the PSD. The energy dispersion in keV/channel was calculated from a least squares analysis of the shifts of the spectral peaks with magnetic field. Because of hysteresis effects and other experimental limitations in measuring very small changes in the A1200 magnetic fields, the spectra in Fig. 2 could not all be placed on the same absolute energy scale. For this reason the spectra are plotted in terms of the energy shift as measured from a zero point that corresponds in each spectrum to the mean of the maxima of the two main peaks.

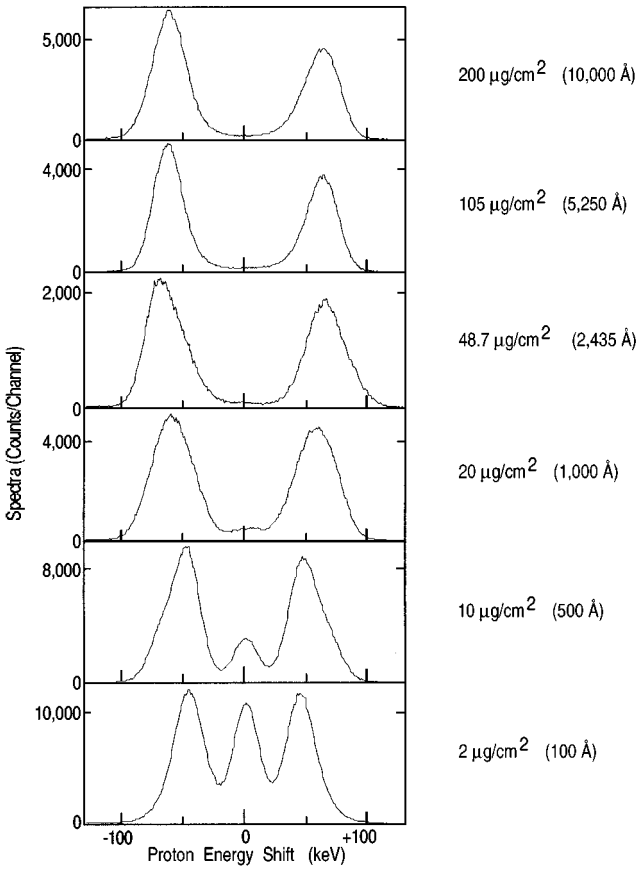

FIG. 2. Energy spectra for protons emerging in the beam direction from carbon foils of various thicknesses (indicated to the right of each spectrum) bombarded by a tightly collimated beam of 173.25-MeV HeH^+ ions. The zero point on the abscissa of each spectrum is located at the mean of the two principal peaks.

The spectra shown in Fig. 2 contain contributions from components that depend on the charge state of the proton's partner helium ion after exit from the foil. (The dwell times range from $\sim 3\times 10^{-17}$ s for the thinnest target to $\sim 3\times 10^{-15}$ s for the thickest and so, as noted above, very little of the Coulomb explosion develops inside the foil.) These components are (i) A ''central peak'' that arises when the partner helium is neutral ($Q_2=0$), (ii) Two peaks corresponding to a singly charged helium partner ($Q_2=1$), and (iii) Two peaks corresponding to a doubly charged helium partner ($Q_2=2$).

The proton peaks corresponding to $Q_2=1$ are seen in the energy spectrum for a 2-μg/cm^2 target, while the peaks corresponding to $Q_2=2$ are seen in the spectra for the two thickest targets (105 and 200 μg/cm^2). For intermediate target thicknesses, the components due to the two helium charge states are mixed in together and not separately resolved.

The central peak is observed only for the thinnest targets and can be ascribed to that fraction of the events in which the incident HeH^+ molecule is collisionally excited into an electronic state that then dissociates into a proton and a neutral helium atom. As the target thickness increases, the electron-loss cross section, which overwhelms the capture cross section at these high energies [15], results in the rapid loss of any neutral helium atoms and the observed protons are then found to be Coulomb-explosion partners to positively charged helium ions. So the central peak disappears rapidly with increasing target thickness. For those cases in which the neutral helium does survive passage through the foil, there is no consequent Coulomb explosion and the protons are observed unshifted in energy and angle (except for very small shifts associated with the small dissociation energies and with stopping power and multiple-scattering effects, as discussed below) from the values they had in the incident projectiles. Thus, unlike the situation for the proton peaks observed in association with charged helium partner ions, the central peak can receive contributions from all initial projectile orientations. This phase-space enhancement results in the central peaks in these energy spectra appearing to be more intense in relation to the actual fraction of dissociations that produce neutral helium fragments.

Small central peaks have been observed at low bombarding energies (for example, with 3.0-MeV HeH^+ bombarding a 195-Å-thick carbon foil [4]). In those cases, however, the production mechanism is quite different. There, the peaks are believed to arise from incident molecular ions whose internuclear spacings happen to be large. These projectiles undergo a very weak Coulomb explosion. Then, multiple scattering and screening effects can result in the fragment pairs emerging from the foil with low velocities relative to one another. At the beam energies used in those measurements there is a small but appreciable probability that the helium ion, which captures and loses electrons rapidly inside the foil, will emerge as a neutral atom and this will result in its partner proton being unshifted (or very nearly so) in energy and angle, thereby contributing to a central peak.

Thus, at the high beam energies of the present work, the central peak in the proton spectrum is due to ''original'' neutral helium atoms (generated near the front surface of the foil), whereas in the low-energy case, it is due to ''reconstituted'' neutral helium atoms formed by electron capture near the back surface of the foil. These two distinctly different mechanisms are akin to those observed in the transmission of fast molecular ions through foils, where one also distinguishes between transmission regimes corresponding to ''original'' and ''reconstituted'' molecular ions [18]. It is to be expected that for the very thin targets there will be a small neutral hydrogen component. In our measurements, we did not seek or detect such fragments.

The energies of the protons emerging from the various foils represented in Fig. 2 may be shifted slightly because of stopping power effects that lead to different energy losses for the different foil thicknesses. However, these effects will be small in relation to the Coulomb-explosion shifts, which are typically several tens of keV. For 35-MeV monatomic proton beams traversing carbon the stopping power is about 15 eV per μg/cm^2 (see, for example, Ref. [19]). Since the protons are part of a cluster, the stopping power will be somewhat higher [10], but even for the thickest targets used in this work, it is safe to assume that the proton energy losses due to stopping (overwhelmingly electronic stopping at these energies) will be well under 10 keV.

Because of the dominance of the electron-loss cross sections [15], referred to above, the equilibrium charge states of the fragments inside the foil correspond to fully stripped H and He ions. These charge states are typically achieved in the

time it takes (~ 1 fs) to traverse a distance in the target material on the order of a few hundred ångstroms (see the discussion of cross sections below). Thus the peak components in Fig. 2 corresponding to $Q_2=2$ ($t_0=0.84$ fs) arise from Coulomb explosions that release their energy essentially entirely after the molecular constituents have reached charge-state equilibrium. That is, during the earlier part of the dissociation when the charge states are changing rapidly, the contribution to the final Coulomb-explosion energy release is negligible. Similarly, the components due to $Q_2=0$ and to $Q_2=1$ ($t_0=1.2$ fs) become unobservably small for foil thicknesses greater than roughly 1000 Å.

The final velocity in the laboratory frame of a proton arising from a projectile Coulomb explosion is given to a good approximation by the vector sum of the initial beam velocity and the asymptotic c.m. velocity, $\overline{u}$, achieved by the proton as a result of the Coulomb explosion. The magnitude of $\overline{u}$ is given by

$$u \approx \sqrt{2\mu Q_1 Q_2 e^2 / M_p^2 r_0}, \tag{4}$$

where M_p is the proton mass. Both the magnitude and direction of the vector $\overline{u}$ will undergo minor modification due to effects such as multiple scattering, stopping, straggling, initial velocity due to the initial momentum distribution, etc. In the vector diagram representing the addition of $\overline{u}$ to the beam velocity, the tip of the vector $\overline{u}$ may be considered as populating with uniform probability the surface of a sphere of radius u, since the incident projectiles are randomly oriented (for a more detailed discussion, see, for example, Ref. [5]). For the protons the magnitude of $\overline{u}$ will depend primarily on the value of Q_2 and on the value of r_0 (for which there is a distribution reflecting the vibrational population in the incoming projectiles).

The vibrational population in the incident beam is unknown. Measurements at low energies on beams from Duoplasmatron and *RF* sources [20] showed that in those cases the ground and low-lying vibrational states are the most populated and that the most probable value of r_0 is about 0.79 Å, the value calculated [21] for the ground state alone. Assuming the same value for r_0 in the present measurement, which uses an ECR source, a simple classical calculation of the energy difference (in the Lab frame) for forward-going and backward-going (in the c.m. frame) protons gives 127 keV for doubly charged helium-ion partners ($Q_2=2$) and 90 keV for singly charged helium-ion partners ($Q_2=1$). Taking relativistic effects into account, these two figures become 129 and 91 keV, respectively. The (laboratory frame) energy differences between the maxima of the two outer peaks shown in Fig. 2 for the 48.7 and 2-μg/cm^2 targets are 133 and 93 keV, respectively. If one assumes that these two spectra are representative of cases for which $Q_2=2$ and $Q_2=1$, then these energy differences clearly indicate that the incident molecular ions are indeed predominantly in the vibrational ground state.

The energy separations of the maxima of the two outer peaks in each spectrum of Fig. 2 are plotted as a function of target-foil thickness in Fig. 3. The plot shows the evolution from predominantly $Q_2=1$ to $Q_2=2$ helium-ion partners (discussed further below). The energy separations can be expected to be slightly modified from the values calculated from the simple model, outlined above, by three main factors:

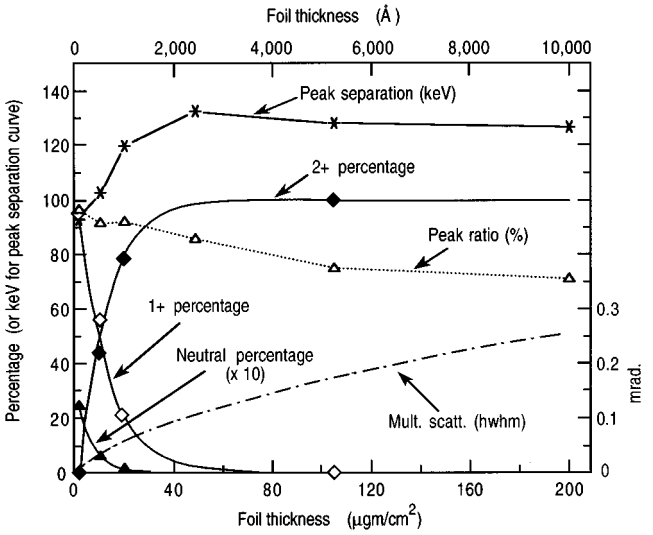

FIG. 3. Plots in terms of target-foil thickness (in μg/cm^2 on the bottom scale, and in ångstroms on the top scale) of several parameters relating to the spectra shown in Fig. 2. Crosses: Peak separation in keV. Open triangles: Ratio of the intensities (at maximum) of the high-energy peak (leading proton) to the low-energy peak (trailing proton) expressed as a percentage. Solid diamonds: Percentage of the emerging protons that have a He^{2+} partner. Open diamonds: Percentage of the emerging protons that have a He^+ partner. Solid triangles: Percentage of the emerging protons that have a He^0 partner. The curves for the three percentages are the best-fit calculations as described in the text. Dot-dashed line: Half-width-at-half-maximum (hwhm) for the angular distribution of multiply scattered monatomic 34.65-MeV protons in carbon (use the scale on the right-hand side).

(i) Phase-space effects. The intensity measured within some small solid angle centered on the beam axis for protons whose *CM* Coulomb-explosion velocity is $\overline{u}$ will be weighted according to u^{-2} (see, for example, Ref. [5]). Thus the larger energy shifts will be reduced in intensity and the most probable value for the peak energy shifts will be correspondingly reduced. Also, the acceptance angle of the A1200 spectrometer was ± 0.2 mrad and this is not completely negligible in relation to the maximum Coulomb-explosion angles of ± 0.65 mrad ($Q_2=1$) and ± 0.92 mrad ($Q_2=2$). This results in an admixture of Coulomb explosions whose energy shifts are slightly less than the maximum and this, in turn, reduces the most probable values of the peak energy shifts.

(ii) Wake effects. A trailing proton experiences a larger rate of slowing down than is the case for a leading proton. Also, the trailing protons experience an aligning force that the leading protons do not. These effects come about (see, for example, Refs. [3] and [5]) because in the trailing case the proton is embedded in the wake of the partner helium ion and thus feels the slowing force exerted by both its own wake and that of the helium ion. When the proton leads, the wake of the helium ion has a much reduced effect on it. Indeed one can see this asymmetry in the energy shifts for the trailing and the leading protons illustrated in the lower

three spectra in Fig. 2 where the central peak is observable and can be taken as a marker for zero energy release in the Coulomb explosion. These effects increase the energy separations for the two outer peaks in the spectra shown in Fig. 2. Wake forces are additionally responsible for the asymmetries in intensity between the trailing and the leading proton peaks as illustrated by the ''peak ratio'' curve in Fig. 3. These asymmetries, also seen at low bombarding energies [2–6], become more pronounced as the target thickness increases, thereby providing longer dwell times during which the wake forces can act.

(iii) Multiple scattering. For increasing foil thicknesses the contribution of multiple scattering to the angular distribution of the emerging protons becomes comparable to both the angular acceptance of the spectrometer and to the maximum Coulomb-explosion angles. As an estimate of the magnitude of this effect the half-width-at-half-maximum (HWHM) for the multiple-scattering angular distribution for a monatomic 34.65-MeV proton beam (isotachic with a 173-MeV HeH^+ beam) penetrating carbon is plotted in Fig. 3. This distribution has a half-width of ± 0.2 mrad (equal to the spectrometer acceptance) when the foil is around 130-μg/cm^2 thick. Multiple scattering has the effect of mixing in Coulomb explosions whose energy shifts are less than the maximum and hence this reduces the energy separations for the two outer peaks in the spectra of Fig. 2. The effect becomes significant for target thicknesses above about 100 μg/cm^2, as is evident from Figs. 2 and 3.

The spectra of Fig. 2 were analyzed to determine the percentages of the proton-producing Coulomb explosions that correspond to the three different charge states of the exiting helium-ion partners. This was done with the following procedure. Characteristic line shapes for each of the five peak types (corresponding to the $Q_2=0$, 1, and 2 components) were determined as follows. First, the spectrum for the 2-μg/cm^2 target was assumed to contain only contributions from $Q_2=0$ (central peak) and $Q_2=1$ (two outer peaks) and the characteristic line shapes for these components were extracted from this spectrum. These peak shapes were then assumed to be characteristic for the central peaks ($Q_2=0$) and for the trailing and leading proton contributions for $Q_2=1$ in all of the spectra. Similarly, the spectrum for the 105-μg/cm^2 target was assumed to contain only contributions from trailing and leading protons associated with $Q_2=2$ partners and these peak shapes were then taken as characteristic for the $Q_2=2$ components in all of the spectra. (The blurring effects of multiple scattering are still small for the 2-μg/cm^2 and the 105-μg/cm^2 targets and were thus ignored at this stage in this analysis.)

These five characteristic line shapes were normalized and then numerically fitted to all six of the spectra of Fig. 2 using a multiple linear regression technique. The resulting 30 fitted distributions (several of which had zero intensity) were then corrected for the u^{-2} phase-space factor (discussed above), multiple scattering, and the effect of the finite experimental angular resolution. (Effects on the ''longitudinal'' energy resolution due to straggling in the target and to the finite resolution of the A1200 spectrometer were negligible. As an aside, the widths of the peaks displayed in Fig. 2 place an upper limit on the energy spread of that part of the cyclotron beam which passed through the tight collimation before the target. The full-width-at-half-maximum of the central peak from the 2-μg/cm^2 target, for example, is about 20 keV which implies a worst-case beam-energy spread from the cyclotron of 20/34, 650 or 6×10^{-4} within the nominally 0.010 in. collimation system used for this experiment.)

The intensities thus determined for the central peaks and the leading peaks were used to determine the percentages of the Coulomb explosions giving rise to protons that had $Q_2=0$, 1, or 2 helium partners. The trailing-proton peaks were not used in this part of the analysis because of the complications of wake effects in the thicker targets. Wake effects, while prominently enhancing the trailing peaks in the longitudinal energy spectrum, actually represent only a small perturbation of the entire 4π phase space and, thus, the leading peaks are considered to be more representative of the yield. The resultant percentages are plotted as functions of target thickness in Fig. 3 for the 2-, 10-, 20-, and 105-μg/cm^2 targets. The data for the 48.7- and the 200-μg/cm^2 targets are omitted from these plots because for the former there appears to have been a slight drift in one or more of the spectrometer magnets during the run, leading to distorted peak shapes, and because for the latter multiple scattering distorts the spectrum.

If we assume that single-electron stripping from the molecular fragments is the overwhelmingly dominant charge-changing process and that double-electron loss can be neglected, then we can create the following set of three simple rate equations for the yields Y_i of the three helium charge states, Q_i,($i=0$,1, and 2) as functions of target thickness:

$$\frac{dY_0}{dx}=-\sigma_l^0 Y_0, \quad \frac{dY_1}{dx}=-\sigma_l^1 Y_1+\sigma_l^0 Y_0, \quad \frac{dY_2}{dx}=\sigma_l^1 Y_1, \tag{5}$$

where σ_l^0 is the cross section for single-electron loss from neutral helium and σ_l^1 is the cross section for single-electron loss from singly charged helium.

The solutions to these equations are

$$Y_0=Y_0(x_m)\exp[-n\sigma_l^0(x-x_m)],$$

$$Y_1=\frac{\sigma_l^0}{\sigma_l^1-\sigma_l^0}Y_0(x_m)\exp[-n\sigma_l^0(x-x_m)] + \exp[-n\sigma_l^1(x-x_m)]\left[Y_1(x_m)-\frac{\sigma_l^0}{\sigma_l^1-\sigma_l^0}Y_0(x_m)\right],$$

$$Y_2=Y_2(x_m)+\frac{\sigma_l^1}{\sigma_l^1-\sigma_l^0}Y_0(x_m)\{1-\exp[-n\sigma_l^0(x-x_m)]\} + \left[Y_1(x_m)-Y_0(x_m)\frac{\sigma_l^0}{\sigma_l^1-\sigma_l^0}\right] \times\{1-\exp[-n\sigma_l^1(x-x_m)]\}, \tag{6}$$

where x_m is the thickness of the thinnest target (the 2-μg/cm^2 target in our case), used for boundary matching conditions, and n is the number of target atoms per unit volume.

The yields shown in Fig. 3 were best-fit with these equations (the fitted curves are shown in the figure) and the helium charge-changing cross sections were extracted. This process gave

$$\sigma_l^0 = 3.55(3)\times 10^{-18}\ \text{cm}^2, \quad \sigma_l^1 = 1.68(6)\times 10^{-18}\ \text{cm}^2. \tag{7}$$

Note that the loss cross section for the two-electron helium is about twice that for the one-electron helium, as one might roughly expect. The errors quoted in Eq. (7) are fitting errors only. The total errors, including systematic effects (e.g., in estimating foil thicknesses, beam-alignment effects, etc.) are assessed at about $\pm 10\%$.

These values may be compared with the estimate given by Bohr [15] for the stripping cross section (low-Z target, high-velocity projectile case),

$$\sigma_{\text{Bohr}} = \pi a_0^2 \frac{4Z_T(Z_T+1)}{Z_P^2}\left(\frac{v_0}{v}\right)^2, \tag{8}$$

where Z_p and Z_T are the atomic numbers of the projectile and target, respectively. This estimate yields $\sigma_{\text{Bohr}} = 2.7\times 10^{-18}\ \text{cm}^2$, slightly higher than the value for σ_l^1 that we determine experimentally.

Katayama *et al.* [22] have measured the charge-changing cross sections for 68-, 99-, and 130-MeV $^3He^{2+}$ ions (22.6, 33.1, and 43.4 MeV per nucleon) traversing carbon. Interpolating their values for σ_l^1 to our beam energy (34.65 MeV per nucleon), gives $1.86\times 10^{-18}\ \text{cm}^2$, in fair agreement with our result and, again, somewhat lower than the Bohr estimate.

Following the treatment of Dennis *et al.* [23], who studied charge exchange for fast ($\beta = 0.36$) $^3He^{2+}$ ions in a variety of materials, we can write the single-electron stripping cross section as

$$\sigma_{\text{strip}} = 8\pi a_0^2 I\left(\frac{v_0}{v}\right)^2, \tag{9}$$

where I is the so-called ''ionization collision strength.''

For the Bohr estimate [Eq. (8)] the collision strength is given by

$$I_{\text{Bohr}} = \frac{Z_T(Z_T+1)}{2Z_P^2}. \tag{10}$$

On the basis of an asymptotic Born-approximation calculation that makes provision for both elastic and inelastic processes in the target atoms, Gillespie [24] has derived a phenomenological expression for the collision strength

$$I_{\text{Gill}} \approx \frac{1.24}{Z_P^2} Z_T(1 + 0.105Z_T - 5.4\times 10^{-4} Z_T^2). \tag{11}$$

Applying this expression to the experimental conditions of the present measurement gives a value of $\sigma_{\text{strip}} = 1.54\times 10^{-18}\ \text{cm}^2$, in reasonable agreement with our measured value of $1.68\times 10^{-18}\ \text{cm}^2$.

IV. CONCLUSIONS

We have reported here measurements on the Coulomb explosion of molecular-ion beams traversing thin carbon foils at significantly higher energies ($\beta = 0.27$) than in previous works. For protons emitted in the beam direction from dissociating HeH^+ projectiles, one clearly sees distinct contributions from the three different charge states of the partner helium fragment. This is the main qualitative difference between these results and those previously found in similar measurements at much lower beam energies. Analysis of the proton energy spectra for various foil thicknesses permits one to extract electron-loss cross sections that are consistent with measurements and calculations on monatomic beams. Evidence for the influences of wake effects and of multiple scattering is noted.

ACKNOWLEDGMENTS

This work was supported by the U.S. Department of Energy, Office of Basic Energy Sciences, under Contract No. W-31-109-ENG-38. We gratefully acknowledge the technical help of B. J. Zabransky, J. P. Greene, and of the staff of the NSCL at Michigan State University.

[1] J. Golovchenko and E. Laegsgaard, Phys. Rev. A **9**, 1215 (1974).
[2] D. S. Gemmell, J. Remillieux, J.-C. Poizat, M. J. Gaillard, R. E. Holland, and Z. Vager, Phys. Rev. Lett. **34**, 1420 (1975).
[3] Z. Vager and D. S. Gemmell, Phys. Rev. Lett. **37**, 1352 (1976).
[4] E. P. Kanter, P. J. Cooney, D. S. Gemmell, K.-O. Groeneveld, W. J. Pietsch, A. J. Ratkowski, Z. Vager, and B. J. Zabransky, Phys. Rev. A **20**, 834 (1979).
[5] D. S. Gemmell, Chem. Rev. **80**, 301 (1980).
[6] P. J. Cooney, D. S. Gemmell, W. J. Pietsch, A. J. Ratkowski, Z. Vager, and B. J. Zabransky, Phys. Rev. A **24**, 746 (1981).
[7] Z. Vager, R. Naaman, and E. P. Kanter, Science **244**, 426 (1989).
[8] Y. Susuki, M. Fritz, K. Kimura, M. Mannami, N. Sakamoto, H. Ogawa, I. Katayama, T. Noro, and H. Ikegami, Phys. Rev. A **51**, 3868 (1995).
[9] H. Raether, in *Solid State Excitations by Electrons*, edited by G. Höhler, Springer Tracts in Modern Physics, Vol. 38 (Springer, Berlin, 1965); R. E. Burge and D. L. Mosell, Philos. Mag. **18**, 251 (1968).
[10] W. Brandt, A. Ratkowski, and R. H. Ritchie, Phys. Rev. Lett. **33**, 1325 (1974).
[11] I. Plesser, Nucl. Instrum. Methods. **194**, 269 (1982).
[12] D. S. Gemmell and Z. Vager, in *Treatise on Heavy-Ion Science*, edited by D. A. Bromley (Plenum, New York, 1985), Vol. 6, p. 243.
[13] P. Sigmund, Phys. Rev. A **46**, 2596 (1992).
[14] D. Zajfman, T. Graber, E. P. Kanter, and Z. Vager, Phys. Rev. A **46**, 194 (1992).
[15] N. Bohr, K. Dan. Vidensk. Selsk. Mat.-Fys. Medd. **18** (8), 1 (1948).
[16] J. A. Nolen *et al.*, in *Proceedings of the 12th International*

Conference on Cyclotrons and Their Applications, edited by B. Martin and K. Ziegler (World Scientific, London 1989), p. 5.
[17] B. M. Sherrill, D. J. Morrisey, J. A. Nolen Jr, and J. A. Winger, Nucl. Instrum. Methods B **56/57**, 1106 (1991).
[18] N. Cue, V. V. de Castro-Faria, M. J. Gaillard, J.-C. Poizat, J. Remillieux, D. S. Gemmell, and I. Plesser, Phys. Rev. Lett. **45**, 613 (1980).
[19] M. J. Berger, International Commission on Radiation Units and Measurements, Report No. 49 (International Commission on Radiation Units and Measurements, Washington, DC, 1993).
[20] E. P. Kanter, D. S. Gemmell, I. Plesser, and Z. Vager, Nucl. Instrum. Methods. **194**, 307 (1982).
[21] See, for example, W. Kolos and J. M. Peek, Chem. Phys. **12**, 381 (1976).
[22] I. Katayama *et al.*, Phys. Lett. **92A**, 385 (1982).
[23] K. Dennis *et al.*, Phys. Rev. A **50**, 3992 (1994).
[24] G. H. Gillespie, Phys. Rev. A **18**, 1967 (1978); **26**, 2421 (1982); see also K. Dennis *et al.*, Ref. [23].